Liquid Crystalline Nanosheet Colloids with Controlled Particle Size Obtained by Exfoliating Single Crystal of Layered Niobate $K_4Nb_6O_{17}$

Nobuyoshi Miyamoto[†] and Teruyuki Nakato*[,†,‡]

PRESTO, Japan Science and Technology Corporation, Japan, and Graduate School of Bio-Applications and Systems Engineering (BASE), Tokyo University of Agriculture and Technology, 2-24-16 Naka-cho, Koganei-shi, Tokyo 184-8588, Japan

Received: August 8, 2003; In Final Form: December 18, 2003

Colloidally dispersed niobate nanosheets with the thickness of 1.8 nm and controlled mean lateral sizes of 0.15−7.8 μm were prepared and their liquid crystallinity was examined. The nanosheet colloids with different lateral sizes were obtained by exfoliation of single crystals of layered niobate $K_4Nb_6O_{17}$ and subsequent ultrasonication. Naked-eye and microscope observations of the nanosheet colloids between crossed polarizers revealed liquid crystallinity of the sols characterized by birefringence as functions of the lateral sizes and concentration of the nanosheets. The nanosheet colloids with smaller lateral sizes (0.15−1.9 μm) varied from isotropic to biphasic (isotropic + liquid crystalline), and finally to fully liquid crystalline states as the colloid concentration increased. The phase transition concentrations (from isotropic to biphasic and biphasic to liquid crystalline) decreased with increasing aspect ratio (lateral-to-thickness ratio) of the nanosheets, almost in accordance with the prediction by Onsager theory, indicating that the liquid crystallinity is explained basically by excluded-volume effect between the nanosheets. On the other hand, the colloids with larger lateral sizes (6.2 and 7.8 μm) stably kept liquid crystalline state even at very low concentration (5.1×10^{-6} in volume fraction), which was much lower than that expected from the theory.

Introduction

Exfoliation of inorganic layered materials into their elementary layers has attracted keen interest in the past decade, because the exfoliated inorganic nanosheets with the thickness of several nanometers and width of up to several micrometers are useful modules for constructing novel nanomaterials. In addition to historically studied clay minerals,[1−10] various layered solids have been exfoliated: chalcogenides,[11,12] phosphates,[13−18] graphite oxide,[19] layered double hydroxides,[20] niobates,[14,16,21−27] titanates,[28−37] and other metal oxides.[38,39] The nanosheets obtained have widely been utilized as modules to fabricate solid nanohybrids by reconstructing the exfoliated nanosheets into cast films,[8,12,23,31,40] layer-by-layer self-assemblies,[9,14−16] electrophoretically deposited films,[33,41] porous solids,[24,29] and nanosheet-polymer composites.[34,42,43] In particular, nanosheets of layered niobates exemplified by $K_4Nb_6O_{17}$, $HTiNbO_5$, and $HCa_2Nb_3O_{10}$, have been paid attention, because of the potential application for advanced materials with the use of their photoactive nature[44−46] and capability of organizing guest species on the layer surface.[47]

We have recently communicated that the colloids of niobate nanosheets prepared by exfoliation of layered niobate $K_4Nb_6O_{17}$ exhibit peculiar liquid crystalline behavior[48] as well as pH-induced sol−gel transition.[49] The nanosheets of $K_4Nb_6O_{17}$ are also interested due to the coiling behavior at low pH to form nanotubules; the dispersed nanotubules also showed liquid crystallinity.[50] Liquid crystallinity of the nanosheet colloids of layered $H_3Sb_3P_2O_{14}$ has also been reported a little while before our finding.[18] These findings demonstrate another novel aspect of the nanosheets other than modules of solid materials, and will lead to rediscovery of the colloidally dispersed inorganic layered materials as soft materials. Inorganic nanosheets may be utilized in colloidal states as novel soft materials with macroscopic alignment; they are distinguished from other assemblies of the nanosheets by their orientationally ordered soft structure.

The liquid crystallinity of the dispersed nanosheets is in particular of great interest both from fundamental aspects and for applications as advanced materials.[18,51,52] Liquid crystalline nanosheet colloids are classified into lyotropic liquid crystals of anisotropic particles with relatively large molecular weights, being distinguished from thermotropic liquid crystals. Theoretical[53−57] and simulation[58−61] studies have verified that colloidally dispersed anisotropic particles (rods and plates) generally form lyotropic liquid crystals because of excluded-volume effects working among the particles. The lyotropic liquid crystals of anisotropic particles are potentially applicable as optical, magnetic, and electric devices,[27,52,62] templates for porous materials,[50,63] soft matrixes of functional molecules,[48] etc.

However, liquid crystallinity of the nanosheet colloids has not been well-understood due to the paucity of systematic studies; only a limited number of colloidal plates have been reported to form liquid crystalline phases, whereas a larger number of colloidally dispersed rods have been found to form liquid crystals: e.g., viruses,[64] chain polymers,[55,65] DNA,[66,67] surfactant micelles, and inorganic nanoparticles.[51,52,62] Nanosheet colloids of natural and synthetic layered clay minerals[1−7] have been studied for long time, and known to form liquid crystalline phases. Nevertheless, they are observed only with gelation of

* To whom correspondence should be addressed. E-mail: tnakat@cc.tuat.ac.jp.

[†] PRESTO, Japan Science and Technology Corporation.

[‡] Graduate School of Bio-Applications and Systems Engineering (BASE), Tokyo University of Agriculture and Technology.

10.1021/jp0363545 CCC: $27.50
Published on Web 04/27/2004

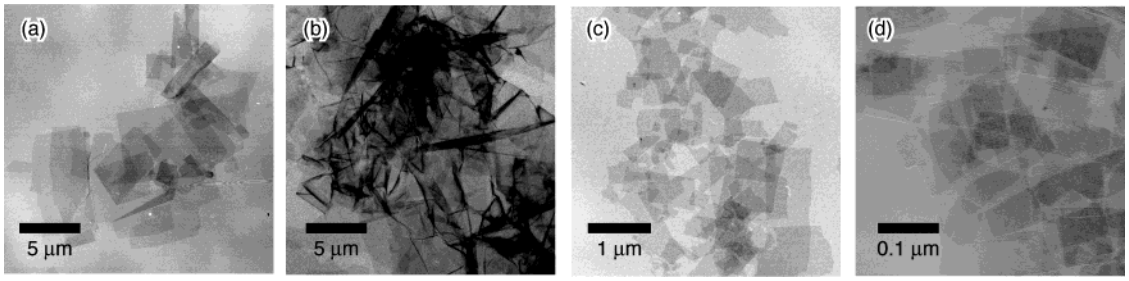

Figure 1. TEM images of the nanosheets obtained from $K_4Nb_6O_{17}$ single crystals after (a)(b) 0, (c) 50, and (d) 180 min of ultrasonication. For the observation (b), the colloid was loaded on the grid without adding methanol.

the colloids; thus details of the clay liquid crystals are still unclear. As another example, colloidally dispersed V_2O_5 nanosheets[68,69] were discovered in 1920s and have been known to show liquid crystallinity; nevertheless, they are recognized as colloids of oblate rods rather than sheets due to the ribbonlike shape with the dimension of e.g., ca. $1 \times 10 \times 1000$ nm^3 of V_2O_5 layers.[70] Recently reported are colloidal plates (not nanosheets) of gibbsite[71,72] and nickel hydroxide,[73,74] characterized by relatively small aspect ratios and low polydispersity; they are used as excellent model systems of theoretical investigations.

In this study, we prepare the nanosheet colloids of exfoliated layered niobate $K_4Nb_6O_{17}$ with controlled lateral size and fixed thickness of 1.8 nm, and demonstrate their liquid crystallinity which is dependent on the lateral size and concentration of the nanosheets. The use of $K_4Nb_6O_{17}$ single crystals as the starting material allows us to control the lateral dimension over an extremely wide range. We have clarified a novel fundamental aspect of colloidally dispersed inorganic nanosheets; it is of significance in manipulating the inorganic layered materials with the delamination technique for constructing various assemblies.

Experimental Section

Preparation of the Niobate Nanosheet Sols with Controlled Particle Sizes by Exfoliation of $K_4Nb_6O_{17}$ Single Crystal. We used single crystals of $K_4Nb_6O_{17}$ as the starting material in order to obtain large nanosheets by exfoliation.[26] $K_4Nb_6O_{17}$ single crystals were prepared by a flux method according to the literature:[75,76] a mixture of K_2CO_3 and Nb_2O_5 (1:1.1 in molar ratio) was heated at 1323 K, and then cooled gradually. The obtained single crystalline $K_4Nb_6O_{17}$ (2−10 mm in width and 1−2 mm in thickness, 5 g) were allowed to react with a 0.2 mmol·dm^{-3} aqueous solution of propylamine hydrochloride at 353 K for 9 d. The reaction product was centrifuged and the deposit was washed three times with water. The obtained wet deposit was redispersed in water (500 dm^3) to form a nanosheet sol ($[Nb_6O_{17}{}^{4-}] = 2.4 \times 10^{-2}$ mol·dm^{-3} or volume fraction $\phi = 6.3 \times 10^{-3}$). The volume fraction ϕ of the sol was calculated according to

$$\phi = [Nb_6O_{17}{}^{4-}]\frac{2acL}{Z}N_A$$

where $[Nb_6O_{17}{}^{4-}]$ is the molar concentration of the niobate, a and c (= 0.76 and 0.64 nm) the lattice parameters of $K_4Nb_6O_{17}$, Z (= 4) the number of $K_4Nb_6O_{17}$ molecules included in its unit cell, L the thickness of nanosheets, and N_A the Avogadro constant. We estimated L as 1.8 nm corresponding to the sum of thicknesses of two $[Nb_6O_{17}]^{4-}$ layers, because $K_4Nb_6O_{17}$ has been reported to be exfoliated with every other interlayer space to form bilayer nanosheets.[22,26]

The nanosheet sol prepared from the single crystals was ultrasonicated for 0, 10, 50, 90, and 180 min to yield the nanosheets with reduced lateral sizes. After the ultrasonication, the concentrations of the colloids were adjusted to $\phi = 5.1 \times 10^{-6} - 2.8 \times 10^{-2}$ by adding or evaporating water (by heating at 353 K). A nanosheet sol was also obtained from powders of $K_4Nb_6O_{17}$,[48] which was prepared by a conventional solid-state reaction, for comparison of the lateral size and for determining the composition of the exfoliated nanosheets.

Characterization of the Nanosheet Sols. Liquid crystallinity of the nanosheet sols was investigated by observing their birefringent nature. The colloids in a test tube or a glass capillary were observed between crossed polarizers and were recorded on a digital camera. Microscope observations of the colloids were carried out with an Olympus BX-51 optical microscope between crossed polarizers.

Transmission electron microscope (TEM) images of the nanosheets in the colloids were taken by using a Hitachi H-7100 microscope operating at 100 kV. A nanosheet sol was added with methanol (water:methanol = 1:9 in volume), and loaded on a grid coated with collodion membrane followed by drying under ambient conditions. When the colloid was loaded without addition of methanol, nanosheets were aggregated on the membrane due to high hydrophobicity of the membrane.

Concentration of the nanosheets was determined by UV spectroscopy using a JASCO Ubest-55 spectrophotometer for concentrated sols obtained after partial evaporation of water. The $[Nb_6O_{17}]^{4-}$ nanosheets showed an absorption band centered at 224 nm with the molar absorption coefficient of 7.6×10^5 mol^{-1} (of $[Nb_6O_{17}]^{4-}$) dm^3 cm^{-1}, being independent of the lateral size of the nanosheets. XRD patterns of the sols after drying on glass plates were recorded on a MAC Science MX Labo diffractometer (monochromatic CuKα radiation). Composition of the powders obtained by evaporating water from the nanosheet colloid (prepared from powders of $K_4Nb_6O_{17}$) was determined by X-ray fluorescence spectroscopy (XRF) using a Rigaku RIX-3100 wave-dispersed X-ray fluorescence analyzer and CHN analysis. The viscosity of the colloid was measured with Ubbelohde-type viscometers.

Results

Formation of the Nanosheet Sols with Controlled Particle Size. Exfoliation of the single crystal of $K_4Nb_6O_{17}$ yielded large niobate nanosheets. Figure 1a shows a typical TEM image of the nanosheets before sonication. Rectangular plates with the lateral sizes of up to ca. 100 μm are observed. Distribution of D, the lateral size, was estimated as Figure 2a by measuring the lengths of the edges of plates observed in the TEM images (over 100 edges were measured). Since D obviously has a log-normal distribution, we estimate the mean lateral size

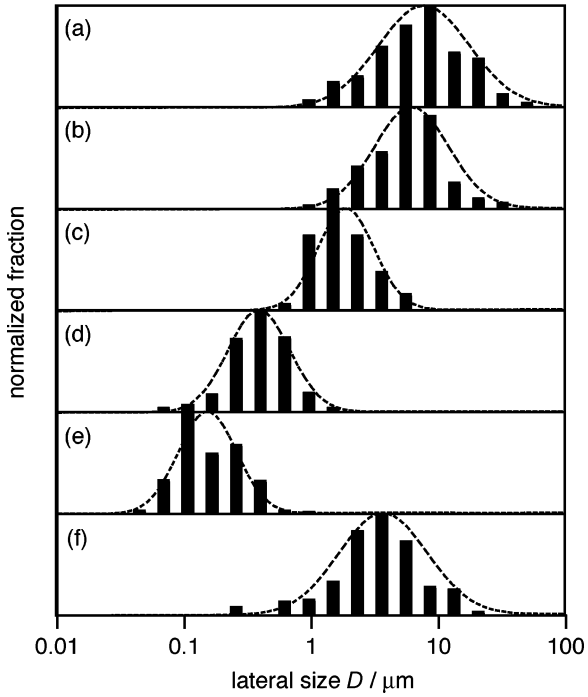

Figure 2. Size distributions of the nanosheets obtained from (a)−(e) single crystals and (f) powders of $K_4Nb_6O_{17}$ with (a) 0, (b) 10, (c) 50, (d) 90, (e) 180, and (f) 0 min of ultrasonication. The dashed lines represent the logarithmic Gaussian distributions with the mean lateral size $D_m = 10^{\langle \log D \rangle}$ and the polydispersity $\sigma_{(\log)} = (\langle(\log D)^2\rangle - \langle \log D\rangle^2)^{1/2}/\langle \log D\rangle$.

TABLE 1: Mean Lateral Sizes and the Critical Concentrations of Phase Transitions

ultrasonication/min	D_m/μm	$\sigma_{(\log)}$/%	$\phi_I{}^a$ (vol/vol)	$\phi_{LC}{}^b$ (vol/vol)
0	7.8	9.2	$<5 \times 10^{-6}$	$\sim 3 \times 10^{-3}$
10	6.2	7.7	$<5 \times 10^{-6}$	$\sim 5 \times 10^{-3}$
50	1.9	6.8	1.9×10^{-3}	1.9×10^{-2}
90	0.38	9.5	7.3×10^{-3}	2.3×10^{-2}
180	0.15	11	1.0×10^{-2}	2.6×10^{-2}
0 (from powder)	3.6	9.8		

[a] The concentration where the colloid transits from isotropic to biphasic. [b] The concentration where the colloid transits from biphasic to liquid crystalline.

D_m and polydispersity $\sigma_{(\log)}$ on the logarithmic scale as $D_m = 10^{\langle \log D \rangle} = 7.8$ μm and $\sigma_{(\log)} = (\langle(\log D)^2\rangle - \langle \log D\rangle^2)^{1/2}/\langle \log D\rangle = 9.2\%$, respectively. This polydispersity corresponds to −56% and +128% on normal scale. In contrast to the nanosheets obtained from single crystal, D_m and $\sigma_{(\log)}$ are estimated as 3.6 μm and 9.8% for the nanosheets from the $K_4Nb_6O_{17}$ powders (Figure 2f), indicating that the difference in starting $K_4Nb_6O_{17}$ affects the lateral size of the exfoliated nanosheets.

Treatment of the sol prepared from single crystalline $K_4Nb_6O_{17}$ with ultrasonication effectively reduced the lateral sizes of the nanosheets. Figure 1c,d shows typical TEM images of the nanosheets obtained by 50 and 180 min of ultrasonication, and Table 1 summarizes D_m and $\sigma_{(\log)}$ of the sonicated sols. The TEM images demonstrate that the nanosheets after sonication possess rectangular shapes similar to those before sonication, while that the lateral size is reduced with prolonged sonication. Figure 2b−e indicates distributions of the lateral size obtained from TEM images for the colloids after 10, 50, 90, and 180 min of sonication, respectively. All of the sols give log-normal distributions similar to that for the as-prepared sol, and D_m is reduced from 7.8 μm to 6.2, 1.9, 0.38, and 0.15 μm after ultrasonication for 10, 50, 90, and 180 min, respectively. $\sigma_{(\log)}$ is kept almost unchanged around 6.8−11%.

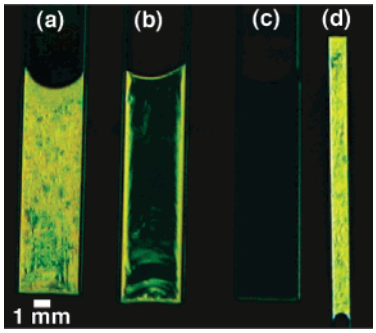

Figure 3. Photographs of the nanosheet colloids with D_m = (a) 7.8 μm, (b) 1.9 μm, and (c)(d) 0.15 μm, and ϕ = (a)−(c) 6.3×10^{-3} and (d) 2.8×10^{-2}. The colloids in flat glass capillaries with the thickness of (a)−(c) 0.4 mm and (d) 0.1 mm were observed between crossed polarizers.

Intrinsic Properties of the Niobate Nanosheets. The TEM observations also give information on intrinsic properties of the niobate nanosheets, the properties which are independent of their lateral sizes. Figure 1b exemplifies flexibility of the nanosheets caused by their thinness. When the sols were mounted on the TEM grids without addition of methanol, the nanosheets are aggregated, bent and crumpled without cleavage, due to high hydrophobicity of the membrane spread on the grid. The flexibility of the $[Nb_6O_{17}]^{4-}$ nanosheets has already been indicated as their coiling to form nanotubules under lowered pHs.[22,26] Flexibility of the nanosheets should affect the behavior of the nanosheets in colloidal states.

The uniformly low contrast of the nanosheets observed in TEM images strongly suggests that all the nanosheets are similar in thickness, probably because of entire exfoliation, regardless of their lateral sizes. In addition, XRD patterns of the films prepared by drying the colloids after 0 and 180 min of the sonication on glass plates (Supporting Information Figure S1) evidence that propylammonium ions are intercalated into every other interlayer space of $K_4Nb_6O_{17}$ to exfoliate the niobate as bilayer nanosheets with the thickness of 1.8 nm.[22,26,77] The composition of the powders recovered by drying the nanosheet colloid (prepared from powdery $K_4Nb_6O_{17}$) is determined as $K_{3.1}(C_3H_7NH_3)_{0.9}Nb_6O_{17}$, also confirming the bilayer structure.

Liquid Crystallinity of the Niobate Nanosheet Sols. Liquid crystallinity of the as-prepared (before ultrasonication) $[Nb_6O_{17}]^{4-}$ nanosheet sols is confirmed by observing them between crossed polarizers. Figure 3a shows a typical photograph of a nanosheet sol before ultrasonication ($D_m = 7.8$ μm; $\phi = 6.3 \times 10^{-3}$ vol.-%) observed between crossed polarizers. The sol clearly shows birefringence. The optical microscope image of the same colloid shown in Figure 4a exhibits textures due to birefringent liquid crystalline domains. Resemblance of the textures to those reported for nematic phases of colloidal plates in the literatures[51,52] suggests that the sol forms a nematic phase, whereas formation of lamellar phase is also possible as is observed for nanosheet colloid of $H_3Sb_3P_2O_{14}$.[18] Occurrence of columnar phase is not probable since it only appears in the colloidal disks with small polydispersity in diameter. Further clarification on the structure of the liquid crystalline sols is now underway by using small-angle neutron scattering and will be published elsewhere.

Images of the colloids between crossed polarizers confirm that the colloids after ultrasonication of 50 min ($D_m = 1.9$ μm) and 180 min ($D_m = 0.15$ μm) also show liquid crystallinity similar to the colloid before sonication. The observations by

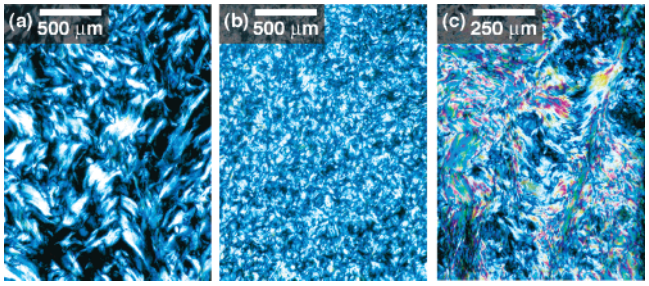

Figure 4. Microscopic images of the nanosheet colloids with D_m = (a) 7.8 μm, (b) 1.9 μm, and (c) 0.15 μm, and ϕ = (a), (b) 6.3×10^{-3} and (c) 2.8×10^{-2}. The colloids were observed between crossed polarizers in the flat glass capillaries with the thickness of (a), (b) 0.2 mm, and (c) 0.1 mm.

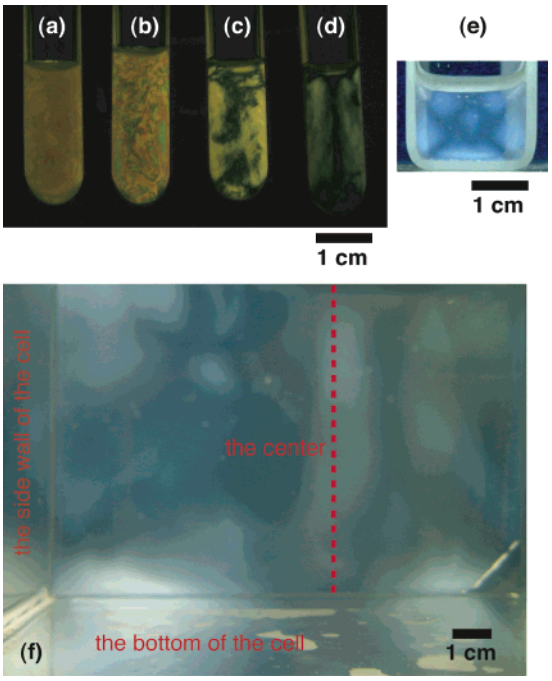

Figure 5. Photographs of the nanosheet colloids (D_m = 7.8 μm) with varied ϕ = (a) 1.5×10^{-3}, (b) 7.6×10^{-4}, (c) 2.5×10^{-4}, (d) 1.3×10^{-4}, and (e)(f) 5.1×10^{-6}. The colloids were observed between crossed polarizers in (a)−(d) a glass tube (1 cm in diameter), (e) a glass cell (10 cm in thickness), and (f) a large glass vessel ($15 \times 15 \times 15$ cm^3).

naked eyes (Figures 3b and d) clearly prove the birefringence of the sols (D_m = 1.9 μm, $\phi = 6.3 \times 10^{-3}$; D_m = 0.15, $\phi = 2.8 \times 10^{-2}$). The microscope images (Figures 4b and c) also characterize the liquid crystallinity of the sols.

Effect of the Particle Size and Concentration of Nanosheets on Liquid Crystallinity. Liquid crystallinity of the niobate sols becomes weaker for the colloids with smaller particles, when compared at a fixed volume fraction of the nanosheets. Figure 3a−c compares the photographs of the nanosheet colloids with the same ϕ (6.3×10^{-3}) and varied D_m observed between crossed polarizers. Although the colloid with D_m = 7.8 μm is strongly birefringent (Figure 3a), the sol with D_m = 1.9 μm is only weakly birefringent (Figure 3b). The sample with D_m = 0.15 μm (Figure 3c) appears wholly dark, indicating that the colloid is isotropic.

The concentration (volume fraction ϕ) of $[Nb_6O_{17}]^{4-}$ nanosheets present in the sols also affected the liquid crystallinity. Figure 5 compares the colloid (D_m = 7.8 μm) at various ϕ, and shows that the observed birefringence becomes weaker as ϕ decreases. Similar trend is found for the sols with other D_m values: for example, the colloid with D_m = 0.15 μm is strongly birefringent at $\phi = 2.8 \times 10^{-2}$ (Figure 3d), whereas the observed interference color becomes weaker with decreasing ϕ, and the colloid is isotropic at $\phi = 6.3 \times 10^{-3}$ (Figure 3c).

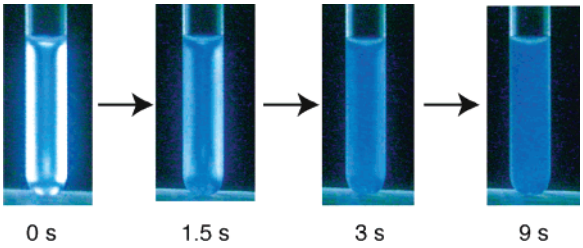

Figure 6. Photographs of the nanosheet colloid (D_m = 1.9 μm, $\phi = 7.6 \times 10^{-4}$) in a glass tube (1 cm in diameter) observed between crossed polarizers during the relaxation process of the birefringent state to isotropic state, induced by rotation of the tube at the rate of approximately 1 revolution per second.

The isotropic sols with rather small D_m or ϕ turned to temporarily birefringent by applying shear stress as exemplified in Figure 6. When the glass tube containing an isotropic sol (D_m = 1.9 μm; $\phi = 7.6 \times 10^{-4}$) is rotated, the colloid become bright along the tube wall between crossed polarizers (Figure 6; 0 s), indicating that the nanosheets are macroscopically oriented along the shear flow. This birefringence is temporal and gradually disappears after terminating the rotation (Figure 6; 1.5−9 s). This result demonstrates that the isotropic phases contain anisotropic particles which are potentially aligned macroscopically by weak external stimuli. We confirmed with observations of some other isotropic samples with different ϕ and D_m that the returning to the isotropic state was slower for the colloids with larger sizes and higher concentrations of the nanosheets.

Liquid Crystalline-Isotropic Biphasic State. We found that the weakly birefringent colloids with rather low ϕ and small D_m, such as the one in Figure 3b, were biphasic mixtures of liquid crystalline and isotropic phases. Figure 7a shows the sol (D_m = 1.9 μm, $\phi = 6.3 \times 10^{-3}$) observed between crossed polarizers before and after phase separation. The colloid is separated into two phases within a day: the birefringent liquid crystalline phase in the bottom and isotropic phase on the upper side. After the separation, the volume of the lower phase was kept almost unchanged even after weeks. We regard the fraction of the birefringent lower phase observed here as the volume fraction of the liquid crystalline phase. UV spectroscopy confirmed that the niobate nanosheets were present in the upper isotropic phase as well as in the lower liquid crystalline phase; concentrations ϕ of the nanosheets in the lower and upper phases were determined as 7.9×10^{-3} and 3.3×10^{-3}, respectively, whereas that of the original colloid was 6.3×10^{-3}. This fact indicates that the observed separation of the colloid is not due simply to settlement nor flocculation of the nanosheets. Similar phase separation behavior was also observed for the colloids with D_m = 0.38 and 0.15 with intermediate concentrations, while the volume fraction of the liquid crystal domain was varied with D_m and ϕ, as will be shown in the next section. Formation of liquid crystalline-isotropic biphasic states and separation under gravitational field due to the difference in the densities are generally observed in the colloidal systems that undergo isotropic to liquid crystalline[18,72] or crystalline[78] phase transitions.

In contrast, the colloids of larger nanosheets (D_m = 6.2 and 7.8 μm) showed more complicated behavior. Figure 7b shows the course of the phase separation of the colloid (D_m = 7.8 μm, $\phi = 1.5 \times 10^{-3}$ vol.-%) observed between crossed polarizers. Although the colloid is separated into the two phases

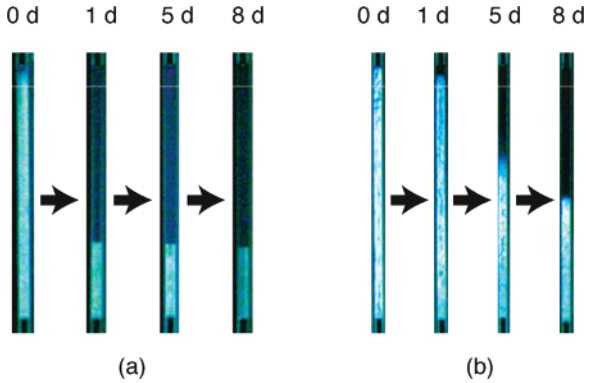

Figure 7. Course of the colloids with (a) $D_m = 1.9\ \mu m$ and $\phi = 6.3 \times 10^{-3}$ and (b) $D_m = 7.8\ \mu m$ and $\phi = 1.5 \times 10^{-3}$ in a glass capillary (0.8 mm in diameter) observed between crossed polarizers.

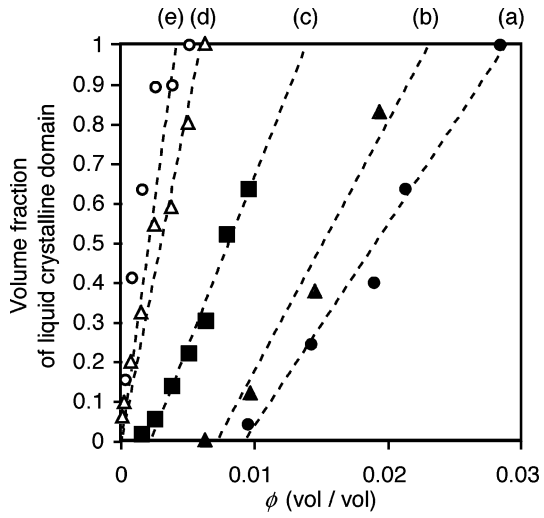

Figure 8. Relationship between colloid concentration ϕ of a colloid and the volume fraction of the liquid crystalline domain to the total volume. The colloids with $D_m =$ (a; filled circle) 0.15, (b; filled triangle) 0.38 and (c; filled square) 1.9 μm were observed 1 d after preparation, whereas the colloids with $D_m =$ (d; open triangle) 6.2 and (e; open circle) 7.8 μm were observed 5 d after preparation.

within 1 d, the volume of the lower phase continued to gradually shrink for more than 10 d. This is probably due to contribution of sedimentation that is not negligible for the colloids of larger nanosheets.[79−81] The colloid with $D_m = 6.2\ \mu m$ also showed similar behavior, whereas the volume fraction of the liquid crystalline domain was smaller compared to the colloid with $D_m = 7.8\ \mu m$ and the same ϕ.

Critical Concentrations of the Phase Transitions. Since the state of the nanosheet colloid varied from isotropic to biphasic, and finally to liquid crystalline as ϕ increased, we determined the critical concentrations of the phase transitions based on the relationship between ϕ and the volume fraction of the liquid crystalline phase. Figure 8a−c shows the relationship observed for the sols with $D_m = 0.15$, 0.38, and 1.9 μm. For each D_m, liquid crystalline domain appears above a certain transition concentration, grows with increasing ϕ, and finally covers whole volume of the colloid. Volume fraction of the liquid crystalline phase is linearly correlated with ϕ. Fitting the plots with straight lines (as shown by dashed lines in the figure) gives intercepts at the volume fraction of the liquid crystalline phase = 0 and 1. The former corresponds to the critical concentration of the phase transition from isotropic to biphasic, ϕ_I, and the latter indicates that from biphasic to liquid crystalline, ϕ_{LC}; they are listed in Table 1. The critical concentrations are lower for the colloids of larger nanosheets, confirming that the colloid of larger nanosheets form more stable liquid crystalline phase.

For the colloids of larger nanosheets ($D_m = 6.2$ and 7.8 μm), the transition concentrations were only roughly determined due to the continuous sedimentation mentioned in the previous section. Figure 8d,e shows the relationships between ϕ and the volume fraction of liquid crystalline phase. We adopted the results after 5 d as the data representing the phase-separated state although the fraction of the liquid crystalline phase significantly varied with time. We estimate that $\phi_{LC} = 5 \times 10^{-3}$ and 3×10^{-3} for the colloids with $D_m = 6.2$ and 7.8 μm, respectively, whereas ϕ_I is nearly 0 for both the systems; namely these sols hardly become isotropic. Observation of the colloid with $D_m = 7.8\ \mu m$ in a glass cell with a long optical path (10 cm) between crossed polarizers gives a little more information of ϕ_I. Weak birefringence is observed for the colloid with $\phi = 5.1 \times 10^{-6}$ as shown in Figure 5e. The colloid with $D_m = 6.2$ μm also kept birefringent at this concentration. Hence, we confirm $\phi_I < 5.1 \times 10^{-6}$ in these systems.

We note that the birefringence observed in these systems is ascribed to permanent liquid crystallinity rather than to temporal ones induced by the gravitational force, interfacial tension, or shear flow. If the nanosheets were oriented along the gravitational force, whole the domain in the vessel should appear bright and dark when the crossed polarizers are set inclined 45° and 0° to the ground, respectively;[48] nevertheless, we did not observe such the phenomenon. By contrast, we have observed birefringent domains oriented along the cell wall (the sides and the bottom) and the liquid surface (Figure 5e). This phenomenon indicates that the orientation of the nanosheets is facilitated at the solid−liquid and air−liquid interfaces. However, observations of the colloids in a large vessel have indicated that the colloids exhibit birefringence without interfacial tension. Figure 5f shows a photograph of a dilute colloid in a large rectangular vessel ($15 \times 15 \times 15\ cm^3$) between crossed polarizers. Domains at the center of the vessel, i.e., far from the cell wall (liquid−solid interface), are also birefringent without macroscopic orientation. Moreover, the effect of shear flow is also excluded. The liquid crystalline colloids kept birefringence even after standing them for more than 2 h, although the shear-induced birefringence of the isotropic colloids (Figure 6) was easily lost after stopping the flow.

Fluidity of the Colloids. The liquid crystalline colloids of the niobate nanosheets examined in the present study retained fluidity, in contrast with the colloids of layered clay minerals whose liquid crystallinity was observed only under gelated state.[5,7] Figures 9a and b show the relationship between the concentration of the niobate nanosheets and kinematic viscosity of the colloids with $D_m = 7.8$ and 0.15 μm. The viscosity of the colloid with $D_m = 0.15\ \mu m$ is as low as the solvent, indicating the high fluidity of the colloid. The viscosity increased at higher concentration and for larger particle size as are generally known behavior of colloidal systems, whereas the colloids here are not gelated over whole the measured concentration range. Eye observation of the sols in a vessel also confirms the fluidity of concentrated colloids; the colloids (e.g., $D_m = 7.8\ \mu m$, $\phi = 1 \times 10^{-2}$) flowed by tilting the vessel. In contrast, according to the literatures, nanosheet colloid of Laponite[5] is gelated at $\phi = 7.2 \times 10^{-3}$. Thus, the sols of niobate nanosheets are less viscous than other known nanosheet colloids.

Discussion

Control of Particle Size by Ultrasonication. This study presents a simple method for controlling the lateral size of

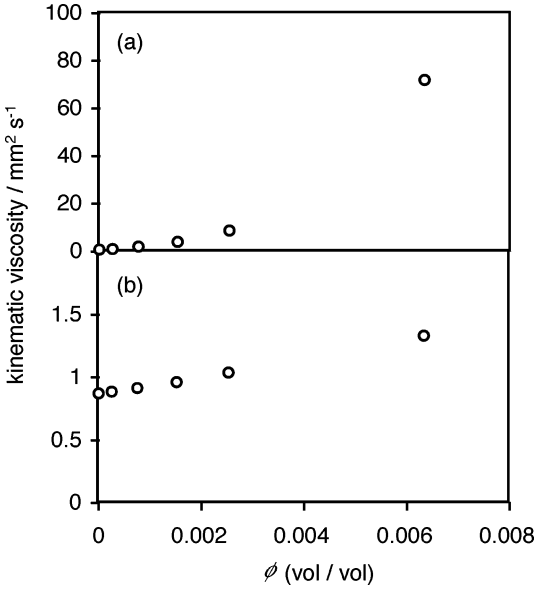

Figure 9. Dependence of kinematic viscosity of the nanosheet colloids with D_m = (a) 7.8 and (b) 0.15 μm on the colloid concentration ϕ. Maximum shear rates at the viscosity measurements are around 30 s^{-1} and 1.6−13 s^{-1} for the colloids with D_m = 0.15 μm and 7.8 μm, respectively.

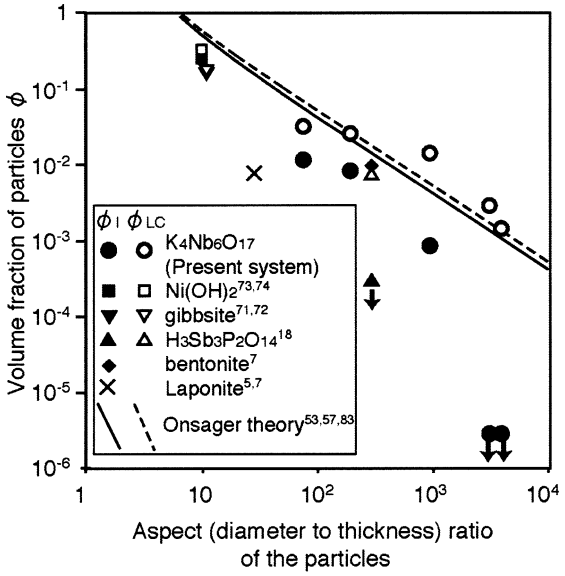

Figure 10. Relationship between diameter-to-thickness ratio of colloidal disks and the transition concentrations ϕ_I (isotropic to biphasic) and ϕ_{LC} (biphasic to liquid crystalline) observed in the present study and in the literatures. Solid and dashed lines represent the theoretical values numerically calculated based on Onsager's second virial approximation.[53,57] The down arrows indicate that the transition concentration was not determined but is lower than the value indicated by the symbols.

inorganic nanosheets prepared by exfoliation of inorganic layered materials. The lateral size of the nanosheets have scarcely been paid attention,[26,35,37] although numerous studies on exfoliation of layered solids have been reported during the past decade. However, the present results demonstrate that the lateral size of the exfoliated niobate layers greatly affects the behavior of colloidally dispersed nanosheets as exemplified by the dependence of the stability of liquid crystalline phase. The lateral size should also be a key factor for controlling optical, electrical and mechanical properties of the nanosheets themselves and the nanohybrid solids obtained by assembling the nanosheets. Since exfoliation of single crystalline $K_4Nb_6O_{17}$ yields large nanosheets, the lateral size of the sheets is easily reduced in a broad range simply by ultrasonication of the as-prepared colloids. This method would be applicable for other layered inorganic materials, whereas polydispersity of the lateral size is still to be controlled.

The distribution of the lateral sizes was log-normal, as commonly found in the size distributions of powder materials.[82] In the present system, this distribution can be explained by a simple model. Supporting Information Figure S2a illustrates the model. If n_i parent sheets having D_i of the edge length are assumed to be broken at the rate of υ into $n_{i+1} = 2n_i$ smaller sheets, whose area is half that of the parent sheets, the distribution of D_i vs n_i is estimated as log-normal when $i \gg 0$ and $t \gg 0$ as shown in Figure S2b.

Origin of the Liquid Crystallinity. The isotropic to liquid crystalline phase transition observed for the niobate nanosheet colloids in the present system is basically rationalized by excluded-volume effect.[53,54] The anisotropic colloids transit from isotropic to liquid crystalline state when the loss of orientational entropy is outweighed by gain in excluded-volume (packing) entropy and, therefore, the liquid crystalline state is favored at higher concentration and larger aspect ratio of the particles.

We compare concentrations of isotropic to biphasic transition ϕ_I and biphasic to liquid crystalline transition ϕ_{LC} observed for the niobate nanosheet colloids in the present study with those of previously reported colloidal systems of inorganic plates and nanosheets: gibbsite,[71,72] Laponite,[5,7] and bentonite[7] exhibit isotropic−nematic phase transition, whereas those $H_3Sb_3P_2O_{14}$[18] and $Ni(OH)_2$[73,74] undergo isotropic−lamellar and isotropic−columnar phase transition. Figure 10 plots ϕ_I and ϕ_{LC} against the aspect ratio of the particles D/L, where D and L are the lateral size and thickness of the inorganic particles, together with the theoretical dependence of ϕ_I and ϕ_{LC} on D/L obtained from the literature[56,57,83] that numerically solved Onsager theory. Except for some cases such as the colloids of niobate with very large D/L ($>10^3$), $H_3Sb_3P_2O_{14}$ and Laponite, the relationship between transition concentrations and aspect ratio is almost in accordance with the theoretical lines for isoropic−nematic transition. This fact demonstrates that the liquid crystalline behavior of the present system as well as the related colloidal nanosheet systems is basically interpreted by the excluded volume effect, although the structure of the liquid crystalline phase (nematic or lamellar) is unclear at present.

Deviations of the experimental ϕ_I and ϕ_{LC} values from the theoretical lines observed in Figure 10 would be explained by the following factors, by which the theory has been extended to be applicable for experimental systems. First, the original theory is not valid at higher concentrations since it only takes into account interactions between two particles; nevertheless, interactions among larger number of particles are not negligible at higher concentrations. The theoretical lines should shift to lower concentrations, if the interactions between many particles are taken into account.[61] Second, the rather large polydispersity in the lateral size observed in present systems would have large effects on the phase transition. Monte Carlo simulations on polydisperse colloidal disks[61] showed that the gap between ϕ_I and ϕ_{LC} is larger at higher polydispersity. Broadening of the gap was also pronounced in the experimental system, colloidal plates of gibbsite.[72] Third, the flexibility of the nanosheet can also affect the liquid crystalline state; theory and experiments on flexible rod (chain polymers) showed that the high flexibility reduce the liquid crystallinity since effective excluded-volume is reduced.[55]

Electrostatic interactions between the nanosheets can also affect the phase behavior; however we suppose that this is not

important in the present system. Electrostatic repulsion among colloidally dispersed particles increases effective diameter of each particle. This leads to increased effective excluded-volume; hence phase transition concentrations become lower.[53,54] However, this effect is not large for disklike particles compared with rods. The excluded-volume is almost independent of the thickness of particle, if Debye screening lengths κ^{-1} is small enough compared to the dimension of a particle.[53,54] For the present system, if diameter and thickness of the particles are enlarged by 50 nm, the transition concentrations ϕ_I are estimated as 100%, 98% and 92% those of the original particles with D = 7.8, 1.9, 0.38 μm, respectively. On the other hand, Debye screening lengths at around ϕ_I of the present systems are estimated as 70, 3.6 and 1.6 nm for the nanosheets with D = 7.8, 1.9, and 0.38 μm, respectively.[84] Judging from these calculations, electrostatic interactions between the nanosheets should be negligible.

On the other hand, the present study indicates that ϕ_I of the sols with very large D/L (the colloid with D_m = 6.2 and 7.8 μm) is significantly smaller than the theoretical value in the order of 2−3. We suppose that restricted motion of colloidal nanosheets due to their large lateral size is a reason for the incompatibility; theoretical and experimental studies have shown that diffusion of anisotropic particles is greatly suppressed for large particles and is anisotropic for plates.[80]

We finally note the effect of gravity on the orientation of the nanosheets. Our observation (Figure 5f) showed that the birefringence observed for dilute colloids of large nanosheets (D_m = 6.2 and 7.8 μm) are due to permanent liquid crystallinity rather than due to gravity-induced sedimentation. In contrast, we have already reported that the liquid crystalline domains of the niobate nanosheets obtained from powders (D_m = 3.6) are macroscopically aligned by gravity at higher concentrations.[48] This apparent discrepancy would be explained based on the calculation of rotary Péclet number, Pe_R, the dimensionless parameter which indicates the effect of gravity to rotational Brownian diffusion.[79,85,86] Brownian diffusion dominates when $Pe_R \ll 1$, whereas the shear flow affect the orientation of the particle when $Pe_R \gg 1$. Pe_R is calculated as 0.082, 0.48, and 0.84 for the nanosheets with D_m = 3.6, 6.2, and 7.8 μm, respectively. These values are not so far from 1 and can vary if the nanosheets interacts with themselves at higher concentrations. Thus, the orientation of these large nanosheets is potentially affected by gravity, depending on the conditions such as colloid concentration.

Conclusions

The present study demonstrate characteristic liquid crystallinity of the colloids of niobate nanosheets depending on the lateral size as well as concentration of the nanosheets. Delamination of single crystalline $K_4Nb_6O_{17}$ enables control of the lateral size over wide range, yielding model platelike particles with very high aspect ratios. The relationship between the aspect ratio and phase transition concentrations (isotropic−biphasic and biphasic−liquid crystalline) indicates that the liquid crystallinity is basically explained by the excluded-volume effect between the nanosheets, being in harmony with Onsager theory of colloidally dispersed anisotropic hard particles. In contrast, the discrepancy between experimental and theoretical phase behaviors at large aspect ratios, probably due to restricted motion of large colloidal particles, represents peculiar behavior of the colloidal systems of the niobate nanosheets.

Because of versatility of liquid crystals, which have been utilized in various areas as, for example, displays, anisotropic reaction media, and templates for ordered nanostructures, liquid crystalline nanosheet colloids will also be applied widely as advanced materials. The high fluidity of the liquid crystals obtained here, in particular for the colloids of large nanosheets which exhibit liquid crystallinity at very low concentrations, distinguishes the present system from conventional liquid crystalline materials; hence, high responsiveness to electric, magnetic and shear stimuli, e.g., gravity induced macroscopic orientation already reported in the previous communication,[48] are expected. Combining the liquid crystallinity with other properties of the layered niobate such as semiconducting nature[44−46] and capability of organizing guest species on the layer surface[47] will lead to integrated materials. Extension of the present methodology to other layered materials such as layered titanates and perovskite-type oxides will provide variety of liquid crystalline colloidal systems which may be useful for both application and fundamental investigations.

Acknowledgment. This work was partly supported by a Grant-in-Aid (No. 14750661) for Young Scientists from the Ministry of Education, Culture, Sports, Science and Technology, Japan.

Supporting Information Available: The XRD patterns of the nanosheet colloids dried on a glass plate (Figure S1, PDF), and the schematic model of breaking down of the nanosheets (Figure S2, PDF). These materials are available free of charge via the Internet at http://pubs.acs.org.

References and Notes

(1) Langmuir, I. *J. Chem. Phys.* **1938**, *6*, 873−896.
(2) van Olphen, H. *An Introduction to Clay Colloid Chemistry*, 2nd ed.; Krieger: Malabar, FL, 1977.
(3) Mourchid, A.; Delville, A.; Levitz, P. *Faraday Discuss.* **1995**, *101*, 275−285.
(4) Mourchid, A.; Delville, A.; Lambard, J.; Lécolier, E.; Levitz, P. *Langmuir* **1995**, *11*, 1942−1950.
(5) Mourchid, A.; Lécolier, E.; van Damme, H.; Levitz, P. *Langmuir* **1998**, *14*, 4718−4723.
(6) Lemaire, B. J.; Panine, P.; Gabriel, J. C. P.; Davidson, P. *Europhys. Lett.* **2002**, *69*, 55−61.
(7) Gabriel, J.-C. P.; Sanchez, C.; Davidson, P. *J. Phys. Chem.* **1996**, *100*, 11 139−11 143.
(8) Ogawa, M.; Takahashi, M.; Kuroda, K. *Chem. Mater.* **1994**, *6*, 715−717.
(9) Kleinfeld, E. R.; Ferguson, G. S. *Science* **1994**, *265*, 370−373.
(10) Inukai, K.; Hotta, Y.; Taniguchi, M.; Tamura, S.; Yamagishi, A. *J. Chem. Soc., Chem. Commun.* **1994**, 959−960.
(11) Murphy, D. W.; Hull, G. W. *J. Chem. Phys.* **1975**, *62*, 973−978.
(12) Lagadic, I.; Lacroix, P. G.; Clément, R. *Chem. Mater.* **1999**, *9*, 22 004−22 012.
(13) Alberti, G.; Casciola, M.; Costantino, U. *J. Colloid Interface Sci.* **1985**, *107*, 256−263.
(14) Keller, S. W.; Kim, H.-N.; Mallouk, T. E. *J. Am. Chem. Soc.* **1994**, *116*, 8817−8818.
(15) Kim, H.-N.; Keller, S. W.; Mallouk, T. E. *Chem. Mater.* **1997**, *9*, 1414−1421.
(16) Kaschak, D. M.; Lean, J. T.; Waraksa, C. C.; Saupe, G. B.; Usami, H.; Mallouk, T. E. *J. Am. Chem. Soc.* **1999**, *121*, 3435−3445.
(17) Yamamoto, N.; Okuhara, T.; Nakato, T. *J. Mater. Chem.* **2001**, *11*, 1858−1863.
(18) Gabriel, J.-C. P.; Camerel, F.; Lemaire, B. J.; Desvaux, H.; Davidson, P.; Batail, P. *Nature* **2001**, *413*, 504−508.
(19) Kotov, N. A.; Dékány, I.; Fendler, J. H. *Adv. Mater.* **1996**, *8*, 637−641.
(20) Adachi-Pagano, M.; Forano, C.; Besse, J.-P. *Chem. Commun.* **2000**, 91−92.
(21) Treacy, M. M. J.; Rice, S. B.; Jacobson, A. J.; Lewandowski, J. T. *Chem. Mater* **1990**, *2*, 279−286.
(22) Saupe, G. B.; Waraksa, C. C.; Kim, H.-N.; Han, Y. J.; Kaschak, D. M.; Skinner, D. M.; Mallouk, T. E. *Chem. Mater.* **2000**, *12*, 1556−1562.
(23) Abe, R.; Hara, M.; Kondo, J. N.; Domen, K. *Chem. Mater.* **1998**, *10*, 1647−1651.

(24) Abe, R.; Shinohara, K.; Tanaka, A.; Hara, M.; Kondo, J. N.; Domen, K. *Chem. Mater.* **1997**, *9*, 2179−2184.
(25) Schaak, R. E.; Mallouk, T. E. *Chem. Mater.* **2000**, *12*, 3427−3434.
(26) Miyamoto, N.; Yamamoto, H.; Kaito, R.; Kuroda, K. *Chem. Commun.* **2002**, 2378−2379.
(27) Osterloh, F. E. *J. Am. Chem. Soc.* **2002**, *124*, 6248−6249.
(28) Sasaki, T.; Watanabe, M.; Hashizume, H.; Yamada, H.; Nakazawa, H. *J. Am. Chem. Soc.* **1996**, *118*, 8329−8335.
(29) Sasaki, T.; Nakano, S.; Yamauchi, S.; Watanabe, M. *Chem. Mater.* **1997**, *9*, 602−608.
(30) Sasaki, T.; Watanabe, M. *J. Am. Chem. Soc.* **1998**, *120*, 4682−4689.
(31) Abe, R.; Shinohara, K.; Tanaka, A.; Hara, M.; Kondo, J. N.; Domen, K. *Chem. Mater.* **1998**, *10*, 329−333.
(32) Kim, J.-Y.; Chung, I.; Choy, J.-H. *Chem. Mater.* **2001**, *13*, 2759−2761.
(33) Sugimoto, W.; Terabayashi, O.; Murakami, Y.; Takatsu, Y. *J. Mater. Chem.* **2002**, *12*, 3814−3818.
(34) Sukpirom, N.; Lerner, M. M. *Chem. Mater.* **2001**, *13*, 2179−2185.
(35) Sukpirom, N.; Lerner, M. M. *Mater. Sci. Eng. A* **2002**, *333*, 218−222.
(36) Ide, Y.; Ogawa, M. *Chem. Commun.* **2003**, 1262−1263.
(37) Tanaka, T.; Ebina, Y.; Takada, K.; Kurashima, K.; Sasaki, T. *Chem. Mater.* **2003**, *15*, 3564−3568.
(38) Schaak, R. E.; Mallouk, T. E. *Chem. Commun.* **2002**, *2002*, 706−707.
(39) Omomo, Y.; Sasaki, T.; Wang, L.; Watanabe, M. *J. Am. Chem. Soc.* **2003**, *125*, 3568−3575.
(40) Isayama, M.; Sakata, K.; Kunitake, T. *Chem. Lett.* **1993**, 1283−1286.
(41) Matsumoto, Y.; Funatsu, A.; Matsuo, D.; Unal, U. *J. Phys. Chem. B* **2001**, *105*, 10893−10899.
(42) Usuki, A.; Kojima, Y.; Kawasumi, M.; Okada, A.; Fukushima, Y.; Kurauchi, T.; Kamigatio, O. *J. Mater. Res.* **1993**, *8*, 1179−1184.
(43) Lagaly, G. *Appl. Clay Sci.* **1999**, *15*, 1−9.
(44) Domen, K.; Kudo, A.; Shibata, M.; Tanaka, A.; Maruya, K.; Onishi, T. *J. Chem. Soc., Chem. Commun.* **1986**, 1706−1707.
(45) Kim, Y. I.; Salim, S.; Huq, M. J.; Mallouk, T. E. *J. Am. Chem. Soc.* **1991**, *113*, 9561−9563.
(46) Kudo, A.; Sakata, T. *J. Phys. Chem.* **1996**, *100*, 17 323−17 326.
(47) Miyamoto, N.; Kuroda, K.; Ogawa, M. *J. Am. Chem. Soc.* **2001**, *123*, 6949−6950.
(48) Miyamoto, N.; Nakato, T. *Adv. Mater.* **2002**, *14*, 1267−1270.
(49) Nakato, T.; Miyamoto, N.; Harada, A.; Ushiki, H. *Langmuir* **2003**, *19*, 3157−3163.
(50) Camerel, F.; Gabriel, J.-C. P.; Batail, P. *Chem. Commun.* **2002**, 1926−1927.
(51) Sonin, A. S. *J. Mater. Chem.* **1998**, *8*, 2557−2574.
(52) Gabriel, J.-C. P.; Davidson, P. *Adv. Mater.* **2000**, *12*, 9−20.
(53) Onsager, L. *Ann. NY Acad. Sci.* **1949**, *51*, 627−659.
(54) Vroege, G. J.; Lekkerkerker, H. N. W. *Rep. Prog. Phys.* **1992**, *55*, 1241−1309.
(55) Sato, T.; Teramoto, A. *Adv. Polymer Sci.* **1996**, *126*, 85−161.
(56) Forsyth, P. A.; Marcelja, S.; Mitchell, D. J.; Ninham, B. W. *J. Chem. Soc., Faraday Trans. 2* **1977**, *73*, 84−88.
(57) Forsyth, P. A.; Marcelja, S.; Mitchell, D. J.; Ninham, B. W. *Adv. Colloid Interface Sci.* **1978**, *9*, 37−60.
(58) Frenkel, D.; Eppenga, R. *Phys. Rev. Lett.* **1982**, *52*, 1089−1092.
(59) Frenkel, D.; Mulder, B. M. *Mol. Phys.* **1985**, *55*, 1171−1192.
(60) Veerman, J. A. C.; Frenkel, D. *Phys. Rev. A* **1992**, *45*, 5632−5648.
(61) Bates, M.; Frenkel, D. *J. Chem. Phys.* **1999**, *110*, 6553−6559.
(62) Li, L.; Walda, J.; Manna, L.; Alivisatos, A. P. *Nano Lett.* **2002**, *2*, 557−560.
(63) Camerel, F.; Gabriel, J.-C. P.; Btail, P. *Adv. Funct. Mater.* **2003**, *13*, 377−381.
(64) Bawden, F. C.; Pirie, N. W.; Bernal, J. D.; Fankuchen, I. *Nature* **1936**, *138*, 1051−1052.
(65) Ciferri, A., Ed. *Liquid Crystallinity in Polymers*; VCH publishers, Inc.: New York, 1991.
(66) Livolant, F.; Levelut, A. M.; Doucet, J.; Benoit, J. P. *Nature* **1989**, *339*, 724−726.
(67) Strzelecka, T. E.; Davidson, M. W.; Rill, R. L. *Nature* **1988**, *331*, 457−460.
(68) Zocher, H. *Z. Anorg. Allg. Chem.* **1925**, *147*, 91−110.
(69) Pelletier, O.; Bourgaux, C.; Diat, O.; Davidson, P.; Livage, J. *Eur. Phys. J. B* **1999**, *12*, 541−546.
(70) Davidson, P.; Garreau, A.; Livage, J. *Liquid Crystals* **1994**, *16*, 905−910.
(71) van der Kooij, F. M.; Lekkerkerker, H. N. W. *J. Phys. Chem. B* **1998**, *102*, 7829−7832.
(72) van der Kooij, F. M.; Kassapidou, K.; Lekkerkerker, H. N. W. *Nature* **2000**, *406*, 868−871.
(73) Brown, A. B. D.; Clarke, S. M.; Rennie, A. R. *Langmuir* **1998**, *14*, 3192−3132.
(74) Brown, A. B. D.; Ferrero, C.; Narayanan, T.; Rennie, A. R. *Eur. Phys. J. B* **1999**, *11*, 481−489.
(75) Kestigian, M.; Leipziger, F. D.; Carter, J. R.; Garabedian, F. G. *J. Am. Ceram. Soc.* **1966**, 517.
(76) Nassau, K.; Shiever, J. W.; Bernstein, J. L. *J. Electrochem. Soc.* **1969**, *116*, 348−353.
(77) Since $K_4Nb_6O_{17}$ possesses alternating two types of interlayer spaces, it can form two type of intercalation compounds: one accommodates the guest species in every other interlayer space and the other contain them in both spaces. The former type of intercalation compounds yields bilayer nanosheets by exfoliation through infinite swelling of the interlayer spaces with the guests, whereas the latter produces monolayer nanosheets. The thickness of the $[Nb_6O_{17}]^{4-}$ nanosheets obtained by exfoliation with tetrabutylammonium[22] or propylammonium[26] has been estimated by using atomic force microscope as around 1.8 nm, which value corresponds to the thickness of the bilayer nanosheets, i.e., total thickness of two $[Nb_6O_{17}]^{4-}$ layers with K^+ sandwiched in the interlayer space.
(78) Pusey, P. N.; van Megen, W. *Nature* **1986**, *320*, 340−342.
(79) Brenner, H. *Int. J. Multiphase Flow* **1974**, *1*, 195−341.
(80) van der Kooij, F. M.; Phillipse, A. P.; Dhont, J. K. G. *Langmuir* **2000**, *16*, 5317−5323.
(81) Russel, W. B.; Saville, D. A.; Schowalter, W. R. *Colloidal Dispersion*; Cambridge University Press: Cambridge, 1989.
(82) Allen, T. *Particle Size Measurement*; Chapman and Hall Ltd.: London, 1968.
(83) Since the literature gives relationship between the aspect ratio D/L and the reduced density ρV_{excl}, where ρ is the number density of the particles and V_{excl} is the excluded volume per one particle. ρV_{excl} is converted to volume fraction ϕ of the particles for comparison with experimental values as $\phi = (\rho V_{excl})(V_{core}/V_{excl})$, where V_{excl} between two cylinders with the diameter D and thickness L is $V_{excl} = (\pi/4)D\{L^2 + [(\pi + 3)/2]LD + (\pi/4)D^2\}$, and the core volume of a disk V_{core} is $V_{core} = (D^2/4)\pi \cdot L$. At isotropic to biphasic transition, ρV_{excl} is estimated as 3.3−5.6 by numerical solution[55,56] for monodisperse colloidal disks with D/L ranging from ∞ to 0.1.
(84) Debye screening length κ^{-1} is calculated as $\kappa^{-1} = \sqrt{\epsilon_0 \epsilon_r k_B T / e^2 N_A 2I}$, where ϵ_0 is permittivity of vacuum, ϵ permittivity of solvent, k_B Boltzmann constant, e the charge of an electron, N_A Avogadro constant, T the temperature, and I the ionic strength of colloid. Ionic strength I is: $I = (1/2)\sum_i c_i z_i^2 = [Nb_6O_{17}{}^{4-}]$, where c and z are the molar concentration and the valence of ions, respectively, if we assume that 1 mol of $[Nb_6O_{17}]^{4-}$ releases 2 mol of monovalent cations (K^+ or popylammonium).
(85) Okubo, T. *J. Am. Chem. Soc.* **1987**, *109*, 1913−1916.
(86) Pe_R for a very thin circular disk with the radius r is expressed as[79,85] $Pe_R = \dot{\gamma}/D_R = 32r^3\eta_0\dot{\gamma}/3kT$, where $\dot{\gamma}$ is the shear rate, D_R the rotational diffusion constant, η_0 the viscosity of solvent, k Boltzmann constant, and T the temperature. On the other hand, the disk sediments at infinite dilution in the gravitational field at the velocity S of $S = V(\rho - \rho_0)g/f$, where g is the gravitational constant, $V (= \pi r^2 L$; L is the thickness of disk) the volume of the disk, ρ and ρ_0 the densities of the particle and the solvent, and f the friction factor. Since f is given as $f = 6\eta_0(2r)$ for a randomly oriented disk with $2r/L \rightarrow \infty$[80] and $\dot{\gamma} = S/(2r)$, we obtain $Pe_R = 4\pi r^3 L(\rho - \rho_0)g/9kT$.